JOURNAL OF SPACECRAFT AND ROCKETS
Vol. 38, No. 4, July–August 2001

Direct Simulation of Apex Enhancement on the Flux onto European Retrievable Carrier

Jingqi Miao*
University of Kent at Canterbury, Canterbury, England CT2 7NR, United Kingdom
and
J. P. W. Stark†
University of London, London, England E1 4NS, United Kingdom

The extended direct simulation Monte Carlo method is employed to model fluxes of meteoroid and space debris onto surfaces of the sun-pointing spacecraft European Retrievable Carrier. Apex enhancement of the Earth motion on flux is considered by including a parameter to describe the anisotropic velocity directionality in the meteoroid distribution. The anisotropy of the measured fluxes onto different surfaces is well explained by this approach, and results are consistent with measured data. Also, the effect of the apex enhancement of the Earth motion on the morphology of the impacts is analyzed, and a good agreement with measured data is achieved. Our simulation allows an estimation of the extent to which the directionality distribution of the meteoroid velocity unit vectors deviates from the isotropic distribution.

Nomenclature

A_s	=	area of a surface of EURECA, m^2
a_s	=	semimajor axis, km
d_i	=	diameter of a particle, m
e_s	=	eccentricity
F_N	=	particle weighting factor
G	=	Earth gravitational constant
i_s	=	inclination, deg
J	=	flux of particles, m^{-2} s^{-1}
$M_\oplus$	=	mass of the Earth, kg
$\boldsymbol{N}$	=	surface normal unit vector
N_{cqp}	=	maximum number of selected pairs between species p and q in a cell
$N_{p(q)}$	=	number of simulated particles of species p (q) in a cell
P	=	probability
R_{am}	=	random number between 0 and 1
r	=	particle altitude, km
t	=	time, s
V_j	=	volume of the jth shell, m^3
v	=	particle velocity, m/s
v_{esc}^2	=	escape velocity of a particle at r from the Earth center, m/s
v_{Rpq}	=	relative velocity of particle p to q, m/s
v_{tot}	=	total velocity of a meteoroid at r from the Earth center, m/s
v_∞	=	velocity of a particle at infinity, m/s
x_i, y_i, z_i	=	xyz components of a particle's position
α	=	parameter used to describe apex enhancement effect
β_i	=	angle between $\boldsymbol{N}$ and v_{Rpq}, deg
γ	=	parameter used when distributing a meteoroid's velocity
Δt	=	simulation time step, s
Θ	=	angle between $\boldsymbol{N}$ and $\boldsymbol{r}$, deg
θ_c	=	half-angle of shielding by the Earth
θ_i	=	latitude angle of a meteoroid in the Earth-centered frame,deg
θ_s	=	true anomaly, deg
σ_{Tpq}	=	total cross section between particle q and p, m^2
φ	=	polar angle of a meteoroid in the Earth-centered frame, deg
Ω_s	=	right ascension of ascending nodes, deg
ω_s	=	argument of perigee, deg

Received 20 October 2000; revision received 20 February 2001; accepted for publication 25 February 2001.

*Lecturer, School of Physical Science.
†Professor, Department of Engineering, Queen Mary and Westfield College.

Introduction

DURING the last decade, the successful retrieval of the Long Duration Exposure Facility (LDEF) spacecraft has boosted the development of various models for the description of natural meteoroid and man-made space debris particles in the near-Earth space environment. The applications of Kessler's (NASA 96) space debris model[1] and Grün's meteoroid model[2,3] have been used to explain many of the measured results from LDEF. Our own direct simulation Monte Carlo (DSMC) model[4,5] differs significantly in its approach. Our DSMC is based on orbit mechanics and statistical mechanics and produces a uniform and self-consistent method to simulate the collision process for both meteoroid and space debris with a spacecraft surface. Our DSMC has predicted fluxes consistent with measured data onto different surfaces of LDEF. In our own previous work and those in Ref. 1–3, an isotropic incident distribution with respect to the Earth's surface has been assumed for meteoroid.[6]

However, a large discrepancy appears when the preceding meteoroid models are used to estimate the flux onto the front side of solar panels of the European Retrievable Carrier (EURECA),[3,7] the largest sun-pointing spacecraft to be retrieved after LDEF. The measured values (for the total flux including meteoroid and space debris) are almost a factor of 10 below the model's predicted meteoroid flux. This discrepancy has previously been attributed to systematic uncertainties in flux measurements.[3] On the other hand, for meteoroid from the isotropic model, a fairly even distribution of impacts for all sides and both the front and the rear of the solar arrays would be expected for EURECA.[7,8] The same holds to a good approximation for space debris impacts. Thus the total fluxes on different surfaces of EURECA should be very similar. However, experimental survey revealed obvious anisotropies and directionality in the measured impact flux onto these different surfaces.[6,8]

There are significant differences between LDEF and EURECA in their flight attitude. The former was gravity gradient stabilized and kept a fixed orientation with respect to the flight direction for all its surfaces; the latter was in a sun-pointing attitude, exposing different surfaces toward the forward direction along the orbit. This typical attitude makes EURECA's surfaces sensitive detectors for anisotropies in the meteoroid and debris environment around the Earth. Particularly evident is an enhancement seen from the direction of the Earth's apex, i.e., the direction toward which the Earth is

moving as it orbits the sun. However, the precise nature of the anisotropy in the meteoroid influx to Earth is difficult to characterize in that not only does meteoroid flux vary with geocentric viewing direction, but also the velocity distribution as a function of viewing direction will change.[6] McDonnell[6] implemented a simplified approach to apex enhancement in the meteoroid flux simulation by "turning" the particle velocity vector to account for the Earth motion and keeping the scalar velocity values unchanged. This method was used to characterize the anisotropic fluxes onto the surfaces of EURECA and explained some of the flux directionality on different sufaces.

In this paper we document the extention of this model to include an apex enhancement factor for capturing the directionality in velocity distribution of meteoroid, caused by the Earth's motion in the solar system, in order to estimate the extent to which the meteoroid environment around the Earth is anisotropic. We also demonstrate further the validity of our DSMC model and investigate the effects of apex enhancement on the meteoroid flux and impact morphology on EURECA's surfaces. The total fluxes onto different surfaces of EURECA are finally calculated.

In the following sections we first present a brief introduction to our extended DSMC model with the inclusion of an apex enhancement parameter α. We omit here the more detailed description of the basic method, which is represented fully in Refs. 4 and 5. We then give the description of meteoroid and space debris in the selected reference frame, as well as the geometry of EURECA. A discussion of the simulated result is carried before the conclusions are drawn in the final section.

Extended DSMC model

DSMC modeling is a probabilistic simulation method that employs a large number of statistically selected simulated particles of the correct physical size, with each simulated particle representing a fixed number F_N of real particles. Simulation is based on the assumption of particle chaos[9] and the requirement of a dilute particle system. The method is able to determine, among other properties of the system, the collision rate between the particles in the system over a period of time. DSMC modeling is essentially a direct simulation of the Boltzmann equation and the procedures for the probabilistic selection of a representative set of collisions based directly on the relations that have formed the basis of kinetic theory for more than a century.[4,10]

The modeling system is established by assigning each simulated particle, at initial time t_0, a position and a velocity vector that follow from the phase space distribution function. A statistical ensemble represented by $\{r_i, v_i\}_t$, $i = 1, 2, \ldots, N$ in phase space, where N is the total number of the simulated particles, is built up to describe the state of the system at some later time t. The evolution of the system is approached by time marching with a step Δt, and the state of the updated system is replaced by $\{r_i, v_i\}_{t+\Delta t}$. The modeling environment is divided into many cells of volume V_j, where j is the index number for the jth cell.

The DSMC modeling process for collision impact in the space environment consists of two main routines: particle propagation and collision probability determination. After the initial state of the system is distributed assuming microscopic chaos,[9] the kinetic theory is then used to move particles between the cells after a reasonable time interval Δt. This time step is selected from a balance, in that it should be small considering the accuracy of tracing a particle's motion but should be relatively large to achieve a consistent computation of collision rate caused by the low population of particles in the low-Earth-orbit (LEO) environment. The particle propagation routine is straightforward and is described more detailed in Ref. 4. It assumes a non-Keplerian nature of orbital evolution. The collision determination routine is important for the extension to our DSMC model and it is outlined in the following steps: 1) calculation of the number of selected pairs in a DSMC cell of volume V_j and 2) determination of a collision.

In the first step the probability of a collision between two particles, with species index p and q respectively, is proportional to the product of their relative speed v_{Rpq} and total collision cross-section σ_{Tpq}. The probability P of collision, between two simulated particles representing F_p and F_q real particles respectively over the time interval Δt, is equal to the ratio of the volume swept out by their total cross section moving at the relative speed between them to the total volume of the cell, i.e.,

$$P = F_N \sigma_{\mathrm{Tpq}} v_{\mathrm{Rpq}} \Delta t / V_j \tag{1}$$

where F_N is the smaller one between F_p and F_q and the relative speed varies with the choice of the collision partners. The maximum number of selected pairs between species p and q from the cell over the time step is

$$N_{\mathrm{cqp}} = \tfrac{1}{2}[N_p \bar{N}_q F_N (\sigma_{\mathrm{Tpq}} v_{\mathrm{Rpq}})_{\max} \Delta t]/V_j \tag{2}$$

Here N_p is the number of simulated particles of species p, and $\bar{N}_q$ is the average number of simulated particles of species q in this cell.

During second step, for every pair of particles which is randomly selected from V_j the product $\sigma_{\mathrm{Tpq}} v_{\mathrm{Rpq}}$ is calculated, and the collision is computed with probability

$$P_c = \frac{\sigma_{\mathrm{Tpq}} v_{\mathrm{Rpq}}}{(\sigma_{\mathrm{Tpq}} v_{\mathrm{Rpq}})_{\max}} \tag{3}$$

and compared with a randomly produced number R_{am}, which is uniformly distributed between 0 and 1. The pair is accepted as a collision event and recorded if

$$P_c \geq R_{\mathrm{am}} \tag{4}$$

If this condition is not met, the collision will be rejected. Initially an estimated value of $(\sigma_{\mathrm{Tpq}} v_{\mathrm{Rpq}})_{\max}$ is set for different species at the beginning of the simulation, but is then updated if a larger value is subsequently found.

In the simulation process, at each time step, particle propagation, the two steps are repeated for every possible pair for all different species groups, for every cell in the system. Each simulation period (e.g., the actual duration of orbital exposure of the spacecraft) is broken down into these time steps. The results from one simulation contribute to an overall ensemble of measurements of collision freqency. Eventually after many such simulations an ensemble average can be obtained (together with appropriate statistics) to provide collision rates for different species groups.

Description of EURECA, Meteoroid, and Orbital Debris in the Simulation

Sporadic meteoroid and space debris in the LEO environment can be considered to be a dilute system of particles caused by their low number density. In general, space debris arrive temporaneously with a random distribution although there may be enhancements in flux that can be traced to a variety of individual breakup events of the larger particles.[11] For meteoroids an isotropic spatial distribution in the LEO environment is assumed. Their individual orbital elements near the Earth are taken to be uniformly distributed at the inital time t_0. Because their geocentric hyperbolic orbits transit the LEO environment in a very short time interval, their orbital evolution has little influence, and we therefore ignore this evolution in our consideration of their collision with a spacecraft.

In the simulation the LEO environment is divided into a group of Earth-centered concentric shells with a width of 50 km, from the surface of the Earth to an altitude of 2050 km. Meteoroids and space debris are grouped by mass into 19 bins, respectively, with equal mass ratio intervals of 10 over the mass range from 10^{-18} g to 1 g. EURECA is treated as a separate orbit particle group.

The way to describe the position and velocity of a meteoroid is different from that of an Earth-orbiting object because the meteoroid's motion is heliocentric and space debris' motion is geocentric. In the following subsections we will represent the distribution of position and velocity of meteoroid in detail.

Positions and velocities are defined in a rotating reference frame centered at the Earth, with the Z axis pointing to the North Celestial Pole, the $X - Y$ plane passing through the equator, with the X axis in the direction of apex of the Earth motion around the sun and the Y axis points to the center of the sun.

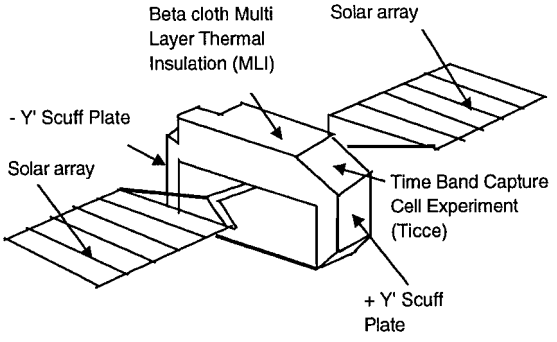

Fig. 1 EURECA spacecraft configuration.

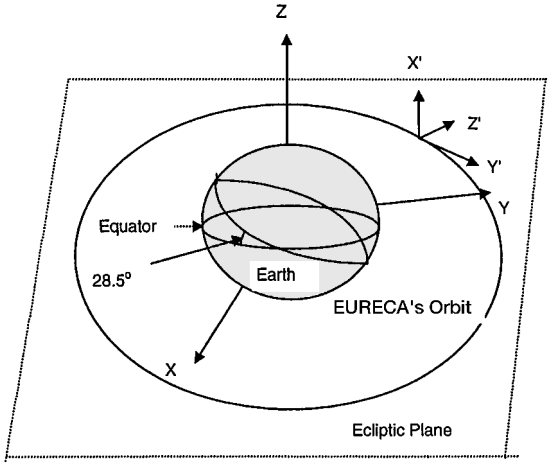

Fig. 2 EURECA pointing geometry.

EURECA Exposure Geometry

Figure 1 shows a sketch of the EURECA spacecraft configuration. The EURECA mission started on 2 August 1992 and was retrieved at altitude of 460 km on 24 June 1993 after being exposed to the space environment for 326 days, starting from an initial orbit of 508 × 502 km and 28.5-deg inclination. We have adopted, as have previous investigators, an orbit for EURECA to be constant at 500 km (Ref. 6).

Throughout its mission, with the exception of maneuver periods, EURECA was in a sun-pointing mode, with the front side of the solar arrays and one face of the spacecraft body ($+Z'$ axis) pointing toward the sun. (See Fig. 1 for a description of the geometry of EURECA in a spacecraft fixed system denoted as X'-Y'-Z'.) The solar arrays were rigidly attached to the main body, i.e., they had no additional degree of freedom.

The long axis of the spacecraft body (Y' axis) was in the orbital plane with the exception of certain brief periods during April and May 1993 when rotations around its Z' axis were performed for experimental purposes.

Unlike LDEF, for EURECA the forward or ram-facing axis varied along the orbit. At local noon the $-Y'$ axis and at local midnight the $+Y'$ axis was facing forward. The $+Z'$ axis (front of solar arrays) was facing forward during the local morning hours and the $-Z'$ axis during the evening. The $+X'$ axis was perpendicular to the orbital plane pointing toward north. A schematic drawing of EURECA in orbit, illustrating EURECA's attitude, is shown in Fig. 2.

Being treated as simply one of the groups of the orbital objects simulated, we use the six Kepler orbital elements to describe EURECA's position in space, i.e., semimajor axis a_s, eccentricity e_s, true anomaly θ_s, inclination i_s, right ascension of ascending node Ω_s, and argument of perigee ω_s. For the orbit parameters of EURECA, we have assumed $e_s = 0.0$, $i_s = 28.5$ deg, and $a_s = r_e + 500$ km, where r_e is the radius of the Earth, and the other three orbit elements θ_s, Ω_s, ω_s were randomly initialized as a result of the long period of orbit evolution considered.

In the defined $X'Y'Z'$ frame the normal unit vector $\boldsymbol{N}$ for the front side of the solar array and body face at $+Z'$ is [0, 1, 0], for the scuff plate at $+Y'$ it is [1, 0, 0], and for the Time Band Capture Cell Experiment (TICCE) surface it is [0, $\sqrt{2}/2$, $\sqrt{2}/2$]. These pointing directions have important consequences for the analysis of anisotropies and directionalities in the measured impact flux.

Space Debris

Each simulated debris particle is expressed by six orbital elements similar to those for EURECA, i.e., $a, e, \theta, i, \Omega, \omega$ evolved with time.

Green et al.[12] developed a space debris size distribution in LEO, which does not differ significantly with inclination or altitude above 200 km. For the altitude range of interest (near the altitude of EURECA), we take this space debris size distribution and change it to mass distribution by a density ρ (Ref. 6).

The inclination and eccentricity distribution of the space debris[4] are introduced to define the initial orbit elements i and e, and the others, a, θ, Ω, and ω are assumed to be uniformly (randomly) distributed for all debris sizes.

During simulation, instead of tracing the trajectory of each space debris and EURECA, each of them is ascribed a most probable location, based on a time-weighted residence.[4] The aerodynamic drag, which causes the semimajor axis a and e to be changed, is included, and the full formulas are adopted from the King-Hele theory.[13]

In the process of cumulating the number of debris collisions for each of EURECA's surfaces, in addition to Eq. (4) no collision is recorded if

$$\pi/4 < \Theta \leq 3\pi/4, \qquad \boldsymbol{v}_i \cdot \boldsymbol{N} \leq 0 \tag{5}$$

or

$$3\pi/4 < \Theta \leq \pi, \qquad \boldsymbol{v}_i \cdot \boldsymbol{N} \geq 0 \tag{6}$$

where Θ is the angle between the surface normal $\boldsymbol{N}$ and the position vector of the ith debris particle relative to the spacecraft and $\boldsymbol{v}_i$ is the relative velocity vector of ith particle. The preceding constrains are caused by the fact that when a particle is in the opposite half sphere to the spacecraft and moves toward the direction against the normal of the surface or when the particle is behind the surface and moves toward the direction of the normal of the surface the particle cannot collide with the surface in the time interval δt, even if Eq. (4) is satisfied.

Meteoroids

Based on Divine's five population interplanetary meteoroid model,[14] combining the Galileo and Ulysses data sets and taking into account the effect of radiation pressure on small particles Grün[15] developed a new meteoroid population model, which provides a very detailed picture of the meteoroid population distribution up to 3 astronomical units (AU) from the sun and of the distribution of their heliocentric orbital elements. For simplicity, we adopt an isotropic total meteoroid concentration distribution[15] with the mass of the meteoroid at 1 AU. This distribution is assumed to be constant with changing altitude in the LEO environment because we are interested in only a narrow altitude range for collisions, relative to the distance between the sun and the Earth. The number of simulated meteoroid particles in each simulation shell can be easily calculated by the product of concentration and cell volumes.

For any simulated meteoroid particle i the spherical coordinate in terms of position r_i, latitude angle θ_i, and polar angle φ_i are randomly distributed, and further the coordinates $\{x_i, y_i, z_i\}$ are obtained by the simple transformation from spherical coordinates to Cartesian coordinates.

Each meteoroid is assumed to approach or leave the Earth on a hyperbolic trajectory[11] with a velocity at infinity of v_∞. The Earth's gravity complicates matters by accelerating the meteoroid toward it, changing its velocity to v_{tot} at a distance r from the center. Conservation of energy demands that v_{tot} be calculable from the initial space velocity and the amount of kinetic energy gained from falling into the Earth's gravitation potential well, i.e.,

$$v_{\text{tot}} = \sqrt{v_\infty^2 + v_{\text{esc}}^2} \tag{7}$$

where v_{esc}^2 is the escape velocity at the distance r from the Earth, which is of the form $v_{esc} = 2GM_{\oplus}/r$, and $r = \sqrt{(x_i^2 + y_i^2 + z_i^2)}$.

The magnitude of velocity v_∞, for every simulated meteoroid particle, was adopted from Taylor's meteoroid velocity distribution,[16,17] which originates from the Harvard Radio Meteor Project data, where about 20,000 meteor observations were taken. Considering that of the total population of meteoroids in the LEO environment at any time t, some will be moving hyperbolically toward the Earth and some will be moving hyperbolically away to return to interplanetary space, we introduce a modulating parameter γ, which is between 0.5 and 1, defined as the ratio of the number of the meteoroids moving toward the Earth to the total number of meteoroids in order to indicate the radial direction of the space velocity of the meteoroids, i.e., for a produced random number R_i of the simulated particle i,

$$v_\infty(i) = \begin{cases} -v & \text{if} \quad R_i < \gamma \quad \text{(toward the center of the Earth)} \\ v & \text{if} \quad R_i > \gamma \quad \text{(away from the center of the Earth)} \end{cases}$$

where v is given a value from Taylor's velocity distribution as just mentioned. If there is no Earth gravity and in the absence of atmospheric drag effects, γ should be 0.5 on average, i.e., each meteoroid only enters the LEO environment briefly, before returning to interplanetary space. A proper value for γ can be found by fitting the simulation results to the observed data. Its deviation from the average value will indicate what portion of meteoroid will not return to interplanetary space after entering the LEO environment as a result of collision with Earth or atmospheric capture. In the following calculations $\gamma = 0.75$ was adopted, which was emprically obtained by fitting LDEF prediction data to measured data.[5]

For the situation of LDEF, the orientation of the meteoroid velocities is described by an uniform distribution over the solid angle 4π because each face of LDEF has nearly equal chance of facing the direction of the apex of the Earth motion, and thus the apex enhancement of the Earth motion has nearly the same effect on its each face. McDonnell[6] reported that inclusion of apex enhancement of the Earth motion resulted in an decreased meteoroid flux onto all of LDEF's faces by 4% on average. Therefore, the effect of apex enhancement of the Earth motion on meteoroid flux onto LDEF's surfaces can be neglected. Unlike the case of LDEF, for EURECA an anisotropic orientation distribution of meteoroid velocities is required to include the apex enhancement effect as a result of its orbital attitude in space as already stated. The direction of the meteoroid velocity thus is assumed to have a bias toward this direction (i.e., X axis in our defined Earth-centered reference frame). In our description of the apex enhancement effect, the scalar velocity distribution of meteoroids is not changed and still follows Taylor's meteoroid velocity distribution in which the velocity already includes the Earth's motion.

Denoting the angle between the ith meteoroid's velocity vector and the X axis as φ_i' ($0 < \varphi_i' < 2\pi$) and introducing a bias parameter α, the probability $P(\varphi_i')$ of φ_i' lying within any unit interval in the the range $[0, 2\pi]$ is $1/2\pi$ for the isotropic direction distribution, but for an anisotropic direction distribution $P(\varphi_i')$ should be larger than $1/2\pi$ in a certain subset of $[0, 2\pi]$ and smaller than $1/2\pi$ in the remainder of $[0, 2\pi]$ in order to keep the normalization of $P(\varphi_i')$ over the interval $[0, 2\pi]$. For example, this subset can be resonably choosen as $[-\pi/4, \pi/4]$, and then the simplest form of the dependence of $P(\varphi_i')$ on α can be written as

$$P(\varphi_i') = \begin{cases} (1/2\pi)(1+\alpha) & \text{if} \quad -\pi/4 < \varphi_i' \le \pi/4 \\ (1/2\pi)(1-\alpha/3) & \text{if} \quad \pi/4 < \varphi_i' \le 3\pi/4 \end{cases} \tag{8}$$

with $\int_0^{2\pi} P(\varphi_i')\, d\varphi_i' = 1$ and $0 \le \alpha < 3$, where α is chosen in such a way that the flux results fit the measured data and $\alpha = 0$ corresponds to an isotropic distribution and $\alpha = 3$ corresponds to the extreme situation that the probability of the orientation of a meteoroid velocity vector in the subset $[-\pi/4, \pi/4]$ is 1, or, in other words, the velocity vectors of all meteoroids are within the cone defined by half angle $\pi/4$ with respect to the X axis. It is obvious that the form of $P(\varphi_i')$ will be different for the various choices of the particle subset.

Therefore we can make a quantitative estimation concerning the extent of the apex bias in the orientation of the meteoroid velocities. Finally the velocity components $\{v_{tot-x,i}, v_{tot-y,i}, v_{tot-z,i}\}$ can be easily obtained by a spherical to Cartesian coordinate transformation.

During the simulation, we do not trace an individual meteoroid's motion over every time step Δt, because the tracing computationally complicates the model; more significantly, however, tracing individual particle's motion is not neccessary because of the short residence time in the LEO environment (as a result of their high approach speed between 20–70 km/s). Isotropy in the meteoroid spatial distribution is assumed for EURECA, and thus it is not necessary to consider the actual meteoroid orbital history.[6] At each time step a new statistical sample is taken from the simulated meteoroid particles with new sets of positions and velocities.

During the simulation, in addition to the condition of Eq. (4), no collision contribution is recorded if 1) the meteoroid cannot impact the surface of EURECA (e.g., $\boldsymbol{r}_i \cdot \boldsymbol{N} < 0$) and 2) the spacecraft is shielded by the Earth. This condition can be considered as follows: a tangent to the Earth's circumference passing through EURECA subtends an angle θ_c with the direction of the Earth's center. Thus the meteoroid cannot strike the spacecraft if approaching from within the cone defined by half angle θ_c, which is given by[18]

$$\sin\theta_c = \frac{r_e\sqrt{v_\infty^2 + v_{esc}^2(r_e)}}{r\sqrt{v_\infty^2 + v_{esc}^2(r)}} \tag{9}$$

where r_e is the radius of the Earth. The term of v_{esc}^2 is from the gravitational focusing effects.

The final point to note during the simulation is that a modification to Eq. (3), which is the form taken for collisions between spherical objects, is needed for an oriented surface with its surface normal not along its direction of motion. Equation (3) is thus redefined to become

$$P_c = \frac{\sigma_{Tpq} v_{Rpq} \cos\beta_i}{(\sigma_{Tpq} v_{Rpq} \cos\beta_i)_{max}} \tag{10}$$

The collisional cross-section area σ_{Tpq} is given by $A_s + \pi d_i^2/4$, with A_s being a surface area of EURECA and d_i the diameter of ith meteoroid, assumed to be spherical, and is related to the meteoroid mass as just noted. During the simulation, we calculate all of the collision frequencies from meteoroid and debris impacts separately on each of EURECA's surfaces.

The ensemble average is used to obtain the average collision number of each species for different faces of EURECA over 100 individual runs with each run simulating the period of 326 days. The values of fluxes are obtained by dividing the average collision number with σ_{Tpq} and the time of 326 days. In the following presentation of results, we denote cumulative flux over the mass range of interest as flux for brevity. The simulations also produce the impact velocity distribution and impact angle distribution, which could be of value in understanding the morphology of the craters caused by these impacts.

Results and Discussion

Fluxes onto the Solar Arrays

The solar arrays are the largest expose surfaces of EURECA with a total area of about 96 m^2. Each wing was made of five panels with dimensions 3.4×1.4 m^2. The dashed line in Fig. 3 is the meteoroid flux on the front side of the solar arrays of EURECA calculated by Staubach's upgraded model.[3] The comparison of that model with EURECA's measured data is clearly disappointing, as can be seen from Fig. 3. After comparing their data with measured total particles flux (circles in Fig. 3), Staubach attributed the significant discrepancy to be caused by systematic uncertainties of particle fluxes obtained from crater counts and associated crater morphology. However their simulated meteoroid flux onto the solar arrays of LDEF can match the measured data very well,[3] which is obtained from the same method of impact crater analysis.[7] It seems that the uncertainties in translating crater size into impactor masses could not be the main reason to cause the discrepancy observable in Fig. 3.

The solid line in Fig. 3 shows the meteoroid flux alone onto the front side of the EURECA's solar arrays calculated in our DSMC

Table 1 Meteoroid flux with different apex enhacement

	log J, m^{-2} s^{-1}		
log mass, g	$\alpha = 0.0$	$\alpha = 1.0$	$\alpha = 1.5$
−1.80E+01	−1.30E+00	−1.35E+00	−1.38E+00
−1.70E+01	−2.29E+00	−2.37E+00	−2.40E+00
−1.60E+01	−3.14E+00	−3.18E+00	−3.20E+00
−1.50E+01	−3.61E+00	−3.67E+00	−3.73E+00
−1.40E+01	−4.28E+00	−4.32E+00	−4.38E+00
−1.30E+01	−5.01E+00	−5.08E+00	−5.14E+00
−1.20E+01	−5.31E+00	−5.39E+00	−5.45E+00
−1.10E+01	−5.51E+00	−5.60E+00	−5.65E+00
−1.00E+01	−5.66E+00	−5.74E+00	−5.81E+00
−9.00E+00	−6.11E+00	−6.20E+00	−6.28E+00
−8.00E+00	−6.36E+00	−6.44E+00	−6.54E+00
−7.00E+00	−7.02E+00	−7.10E+00	−7.19E+00
−6.00E+00	−7.92E+00	−8.01E+00	−8.12E+00
−5.00E+00	−8.63E+00	−8.72E+00	−8.82E+00
−4.00E+00	−9.62E+00	−9.74E+00	−9.84E+00
−3.00E+00	−1.09E+01	−1.09E+01	−1.10E+01
−2.00E+00	−1.22E+01	−1.22E+01	−1.24E+01
−1.00E+00	−1.32E+01	−1.34E+01	−1.35E+01

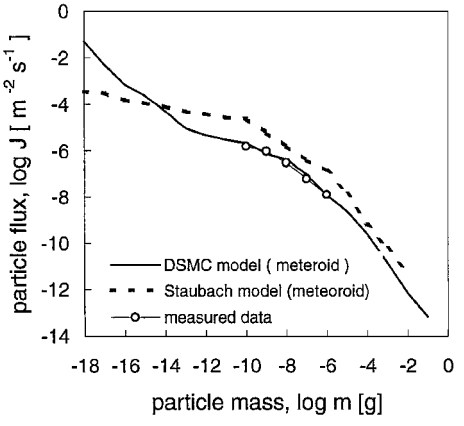

Fig. 3 Fluxes onto the front side of the solar array of EURECA without apex enhancement (meteoroid only).

simulation without including the apex enhancement (i.e., $\alpha = 0$). This result appears consistent with the measured total flux data; however, the underlying assumption is that only a small contribution is from orbital debris for the mass range associated with this data. This assumption seems possible, given reference models for meteoroid[2] and space debris.[19]

The DSMC model without apex enhancement predicts very similar meteoroid fluxes onto both the rear and front sides of the solar arrays. Again similar meteoroid fluxes are predicted for the $\pm Y'$ surfaces of EURECA body. There is no apparent difference between $\pm X'$ surfaces and $\pm Z'$ surfaces. This is not surprising for the assumed isotropic velocity oritentation model with the Earth shielding on one part of the orbit being mirrored on the opposite part. Nevertheless, the measurements of particle fluxes onto the pair of surfaces of opposite orientations gave us significantly different data.[6,8] This inconsistancy between model prediction and measured results is almost certainly a consequence of the real meteoroid environment having anisotropies.[20] We can therefore investigate the quantifiable predictions of flux variations through various values for the anisotropy factor α as a result of the apex enhancement effect from the apex motion of the Earth.

The calculation results of meteoroid fluxes onto the front side of the solar arrays, with different values of α are listed in Table 1. It is shown that the meteoroid flux onto the front side of solar arrays decreases with increase of the apex effect. The flux decreases by 17% on average with the value of α increasing from 0 to 1, i.e., the probability of a meteoroid particle's velocity vector lying in the angular range of $[-\pi/4, \pi/4]$ with respect to the X axis increases from 0.25 to 0.5. This result is quite reasonable on the basis of our apex enhancement model because the normal of the front side of

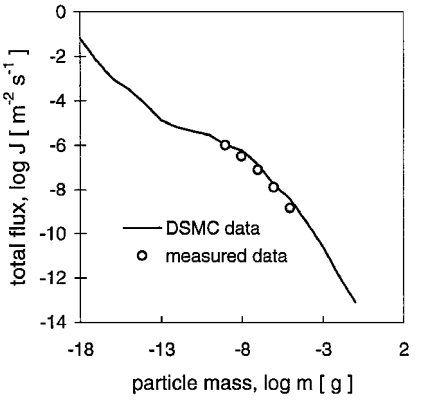

Fig. 4 Total particle flux onto the front side of the solar array of EURECA. (DSMC model with apex enhancement factor α = 1. J is the sum of meteoroid flux and space debris flux.)

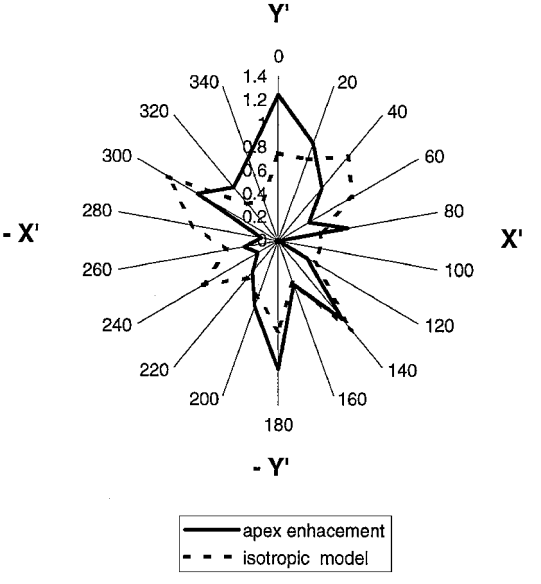

Fig. 5 EURECA solar array directionality (front side).

the solar array is pointing to the sun $(+Y)$, which is perpendicular to the apex direction of the Earth motion $(+X)$. If the velocities of meteoroid particles have a bias toward the X axis, away from the normal of the front side of the solar array the chance for these particles to collide with the front side will decrease, which clearly decreases the flux onto the front side of the solar array.

The preceding result will enable further consideration of the earlier results shown in Fig. 3. We can now evaluate the total flux onto a surface with the meteoroid flux modulated by the apex angle factor α. Figure 3 shows that the DSMC-modeled meteoroid flux (with $\alpha = 0$) is almost equal to the measured total flux data, and it is worrying that the inclusion of space debris will result in an overpredicted total particle flux onto the front side of the solar array. However, we can now expect that the contribution from the space debris could be partly balanced by a decrease in meteoroid flux resulting from apex enhancement. In Fig. 4 the DSMC-modeled total particle flux agrees with measured data very well; here the meteoroid flux is calculated with the apex enhancement factor $\alpha = 1.0$, and the space debris flux is calculated in the way already described.

Figure 5 shows the directionality distribution of the recored impacts on the front side of solar array on EURECA during DSMC modeling. The solid line represents the result for apex enhancement factor $\alpha = 1.0$ and the dashed line for the isotropic meteoroid model with $\alpha = 0.0$. It is evident that there is a significant bias toward the $+Y'$ (X) Earth apex direction, which is consistent with the same picture from experimental measurements.[20]

One of the more surprising results of the EURECA impact investigation was the large number of craters that show signs of ellipicity.

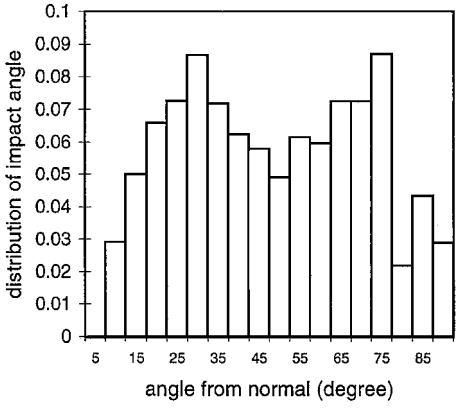

Fig. 6 Impact angle distribution for front side of the solar array.

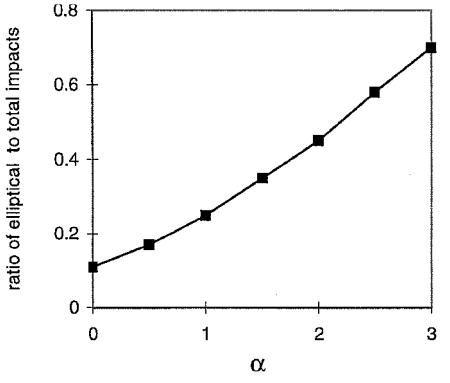

Fig. 7 Ratio of elliptical impacts to total impacts onto the front side of the solar array.

A total of 221 of the 703 impacts analyzed in detail on the front side of the solar array show signs of an impact at an inclined angle.[8] During DSMC modeling, the morphology of the impact can be studied by the recorded impact angles. Figure 6 shows the simulated impact angle distribution for the situation of $\alpha = 1.0$. According to the experimental simulation result reported by Berthaud and Mandeville,[21] when the impact angle is larger than 60 deg the crater is obviously elliptical, and when the impact angle is larger than 80 deg the decapitation effect appears. From the impact angle distribution it suggests that 30.1% of impacts occur with impact angles lying within a cone of 60–80 deg from the normal. This result is consistent with the measured value $\frac{221}{703} \times 100\% = 31.4\%$ (Ref. 8). Figure 7 shows the dependence of impact morphology on the apex enhancement factor α. It is seen that the ratio of elliptical impacts to total impacts increases with the variation of the extent of the apex enhancement effect. The ratio is at its best fit to the experimental measurements.

From both Figs. 6 and 7 we see that when $\alpha = 1$ both the impact flux and the ratio of elliptical impacts to total impacts on the front side of the solar array match with the measured data very well. We will use $\alpha = 1$ in the following calculations.

An investigation of the meteoroid flux onto the rear side of solar array has also been carried out. The results show that the ratio of meteoroid flux onto the front side with respect to rear side rises from 1 to 1.15, when the probability of the velocity vector of a meteoroid particle lying the interval of $[-\pi/4, \pi/4]$ doubles from 0.25 to 0.5 (i.e., α varies from 0 to 1). It means that the meteoroid flux onto the front side decreases more slowly with the increase of the apex enhancement of the Earth than that onto the rear side as a result of the fact that the front side faces forward when the spacecraft moves towards the apex; the relative collision velocity of an apex enhancemented meteoroid to the front side is always higher than that to the rear side.

This ratio is similar to McDonnell et al.'s resulting ratio of 1.17, which is from their apex enhancement simulation. The comparison with measured data is not available because the rear side panels are covered by Kapton foils or other more ductile materials so that only impacts from much larger particles are visible.

Table 2 Meteoroid flux onto $+Y'$ scuff plate with different apex enhancements

	log J, m^{-2} s^{-1}		
log m, g	$\alpha = 0.0$	$\alpha = 1.0$	$\alpha = 1.5$
−1.80E+01	−1.26E+00	−1.23E+00	−1.21E+00
−1.70E+01	−2.25E+00	−2.24E+00	−2.21E+00
−1.60E+01	−3.06E+00	−3.04E+00	−3.02E+00
−1.50E+01	−3.55E+00	−3.53E+00	−3.52E+00
−1.40E+01	−4.21E+00	−4.18E+00	−4.17E+00
−1.30E+01	−4.97E+00	−4.93E+00	−4.91E+00
−1.20E+01	−5.27E+00	−5.23E+00	−5.21E+00
−1.10E+01	−5.46E+00	−5.43E+00	−5.42E+00
−1.00E+01	−5.61E+00	−5.58E+00	−5.57E+00
−9.00E+00	−6.06E+00	−6.03E+00	−6.01E+00
−8.00E+00	−6.31E+00	−6.28E+00	−6.27E+00
−7.00E+00	−6.95E+00	−6.93E+00	−6.92E+00
−6.00E+00	−7.83E+00	−7.84E+00	−7.83E+00
−5.00E+00	−8.57E+00	−8.52E+00	−8.50E+00
−4.00E+00	−9.57E+00	−9.52E+00	−9.50E+00
−3.00E+00	−1.07E+01	−1.08E+01	−1.07E+01
−2.00E+00	−1.22E+01	−1.20E+01	−1.19E+01
−1.00E+00	−1.33E+01	−1.32E+01	−1.32E+01

Table 3 Meteoroid flux onto $\pm Y'$ scuff plate

	log J, m^{-2} s^{-1}	
log m, g	$+Y'$	$-Y'$
−1.80E+01	−1.23E+00	−1.36E+00
−1.70E+01	−2.24E+00	−2.37E+00
−1.60E+01	−3.04E+00	−3.16E+00
−1.50E+01	−3.53E+00	−3.67E+00
−1.40E+01	−4.18E+00	−4.32E+00
−1.30E+01	−4.93E+00	−5.06E+00
−1.20E+01	−5.23E+00	−5.36E+00
−1.10E+01	−5.43E+00	−5.56E+00
−1.00E+01	−5.58E+00	−5.71E+00
−9.00E+00	−6.03E+00	−6.16E+00
−8.00E+00	−6.28E+00	−6.42E+00
−7.00E+00	−6.93E+00	−7.08E+00
−6.00E+00	−7.84E+00	−7.96E+00
−5.00E+00	−8.15E+00	−8.28E+00
−4.00E+00	−8.62E+00	−8.76E+00
−3.00E+00	−9.10E+00	−9.24E+00
−2.00E+00	−9.58E+00	−9.72E+00

Fluxes onto EURECA Body Surfaces

The external surfaces of the EURECA body are mainly covered by thermal multilayer insulation (MLI) blankets, which limited the smallest detectable impact features to about 100 μm ($\sim 10^{-6}$ g). Thus we are not able to compare the absolute value of the predicted particle flux with the measured data, but instead we concentrate on discussions about the apex enhancement effects on the meteoroid flux onto different surfaces.

Listed in Table 2 are DSMC predicted meteoroid fluxes onto the scuff plate ($+Y'$) pointing in the apex direction of the Earth motion ($+X$ in our reference frame). It is seen that with the increasing apex effect factor α, i.e., an increasing directionality of the velocity vector of meteoroid particle in the apex direction of the Earth motion, the fluxes onto the $+Y'$ scuff plate gradually increase because of the higher effective impact velocity when the meteoroid's incident angle has a bias toward the surface normal.

This effect of apex enhancement on the fluxes onto the $+Y'$ scuff plate is opposite to that onto the solar array surface. The flux increases by about 9% when the probablity of the velocity vector of the meteoroid lying within the half-angle of $\pi/4$ to the X axis doubles from 0.25 to 0.5. The same calculation for the $-Y'$ scuff plate gives a decreased meteoroid flux because of the lower effectiveness of impact velocity due to a meteoroid's incident angle bias away from the surface normal; these results are given in Table 3, where the apex effect factor was $\alpha = 1.0$. The ratio of flux onto $+Y'$ with

Table 4 Meteoroid flux on body surfaces of EURECA

	log J, $m^{-2}s^{-1}$		
log m, g	$Y'(+)$	TiCCE	$Z'(+)$
−1.80E+01	−1.23E+00	−1.27E+00	−1.32E+00
−1.70E+01	−2.24E+00	−2.29E+00	−2.35E+00
−1.60E+01	−3.04E+00	−3.08E+00	−3.13E+00
−1.50E+01	−3.53E+00	−3.58E+00	−3.63E+00
−1.40E+01	−4.18E+00	−4.23E+00	−4.28E+00
−1.30E+01	−4.93E+00	−4.98E+00	−5.03E+00
−1.20E+01	−5.23E+00	−5.28E+00	−5.33E+00
−1.10E+01	−5.43E+00	−5.48E+00	−5.53E+00
−1.00E+01	−5.58E+00	−5.63E+00	−5.68E+00
−9.00E+00	−6.03E+00	−6.08E+00	−6.14E+00
−8.00E+00	−6.28E+00	−6.33E+00	−6.39E+00
−7.00E+00	−6.93E+00	−6.98E+00	−7.03E+00
−6.00E+00	−7.84E+00	−7.88E+00	−7.93E+00
−5.00E+00	−8.52E+00	−8.57E+00	−8.62E+00
−4.00E+00	−9.52E+00	−9.58E+00	−9.64E+00
−3.00E+00	−1.08E+01	−1.08E+01	−1.08E+01
−2.00E+00	−1.20E+01	−1.21E+01	−1.22E+01
−1.00E+00	−1.32E+01	−1.33E+01	−1.34E+01

respect to $-Y'$ rises from 1 to 1.4, when the directionality distribution of meteoroid approaching velocities varies from isotropy ($\alpha = 0$) to a bias to the apex of the Earth motion with the factor $\alpha = 1$. The measured corresponding impacts ratio between the two scuff plates is $\frac{16}{6} = 2.6$. We can reasonably attribute this difference to the uncertainty in measured data caused by the property of its covering material and small surface area which result in very limited impacts being measured.[8]

The investigation of the meteoroid flux onto $+Z'$ MLI surfaces reveals very similar values to those for solar array, with the same response to the change of the apex enhancement effect caused by their same surface pointing direction.

The calculation predicts an intermediate meteoroid flux onto the TICCE surface, which points between the X and Z axis in our defined reference frame. Table 4 expresses the meteoroid fluxes onto the surfaces with different pointing directions. The calulation was carried out with $\alpha = 1$. It is shown that because of different apex enhancement effects on different directional surfaces the fluxes exhibit significantly different values onto different directional surfaces as reported in experimental measurements.[6]

Conclusions

The application of our DSMC model to the spacecraft EURECA reveals that the meteoroid plays a dominant part in the cumulative flux onto EURECA's surfaces at least in the particle mass range 10^{-18} to 10 g. The inclusion of apex enhancement of the Earth motion is important to explain the anisotropy in the fluxes onto differently oriented surfaces and the morphology characteristics on the solar array surface.

It is shown that our apex enhancement model of the Earth motion produces different effects on the meteoroid flux onto surfaces with different orientation. The apex enhancement decreases the meteoroid impact rate to the $+X'$ solar array surface and the $+Z'$ MLI surface but increases the meteoroid impacts onto the $+Y'$ scuff plate.

The simulation of total particle flux onto solar arrays exhibits excellent agreement with the measured data. Furthermore, the apex enhancement results in demonstrably different meteoroid flux onto both $\pm Y'$ scuff plates and onto $+X'$, $+Y'$, $+Z'$ surfaces. All of the simulated results are consistent with the experimental measurements.

The inclusion of apex enhancement effects also predicts a much larger number of elliptical impacts onto the front side of solar array than that onto LDEF lateral surfaces, where only 11.7% of impacts are elliptical. The corresponding ratio for EURECA's front side of the solar array is about 30.1%, which matches the measured data very well.

These results show the success of the DSMC model's application to predict the particle flux onto differently oriented surfaces of EURECA and the morphology of the impacts onto the front side of the solar array. Finally we can conclude that the apex enhancement effect from the Earth's motion around the sun doubles the probability of a particle approaching from the apex direction.

Acknowledgment

This work is supported by the Engineering and Physical Science Research Council.

References

[1]Kessler, D. J., Zhang, J., Matney, M. J., Eichler, P., Reynolds, R. C., Anz-Meador, P. D., and Stansbery, E. G., "A Computer-Based Orbital Debris Environment Model for Spacecraft Design and Observations in Low-Earth Orbit," NASA TM 104825, Oct. 1996.

[2]Grün, E., Zook, H. A., Fechtig, H., and Giese, R. H., "Collisional Balance of the Meteoritic Complex," *Icarus*, Vol. 62, May 1985, pp. 244–272.

[3]Staubach, P., Grün, E., and Jehn, R., "The Meteoroid Environment near Earth," *Advances in Space Research,* Vol. 192, No. 1, 1997, pp. 301–308.

[4]Wang, L., and Stark, J. P. W., "Direct Simulation of Space Debris Evolution," *Journal of Spacecraft and Rockets*, Vol. 36, No. 1, 1999, pp. 114–123.

[5]Miao, J., and Stark, J. P. W., "Direct Simulation of Meteoroids and Space Debris Flux on Spacecraft Surfaces," *Planetary and Space Science* (to be published).

[6]McDonnell, J. A. M., "Meteoroid and Debris Flux and Ejecta Models," ESA, Final Rept. 11887/96/NL/JG, Kent, England, U.K., Dec. 1998.

[7]Dauba, O., and Drolshagen, G., "Meteoroids and Debris Flux Predictions for EURCA, the HUBBLE SPACE TELESCOPE, and LDEF," European Space Research and Technology Centre, WP, 1995.

[8]Drolshagen, G., McDonnell, J. A. M., Stevenson, T. J., Deshpande, S., Kay, L., Tanner, W. G., Mandeville, J. C., Carey, W. C., Maag, C. R., Griffiths, A. D., Shrine, N. G., and Aceti, R., "Optical Survey of Micrometeoroid and Space Debris Impact Features on EURECA," *Planetary and Space Science*, Vol. 44, April 1996, pp. 317–340.

[9]Stark, J. P. W., "Evolution of Debris Clouds to Microscopically Chaotic Motion," *Journal of Spacecraft and Rockets*, Vol. 38, No. 4, 2001, pp. 554–562.

[10]Bird, G. A., *Molecular Dynamics and Direct Simulations of Gas Flows*, Oxford Univ. Press, Oxford, 1994, pp. 219–255.

[11]Love, S. G., and Brownlee, D. E., "Heating and Thermal Transformation of Micrometeoroid Entering the Earth's Atmosphere," *Icarus*, Vol. 89, Jan. 1991, pp. 26–43.

[12]Green, S. F., Deshpande, S. P., and Machay, N. G., "A 3-D Numerical Model for Space Debris and Interplanetary Dust Flux Incident on LDEF," *Advances in Space Research*, Vol. 13, No. 8, 1993, pp. 107–110.

[13]King-Hele, D. G., *Satellite Orbits in an Atmosphere: Theory and Application*, Blackie, Glasgow, Scotland, U.K., 1987, Chaps. 4–6, pp. 44–108.

[14]Divine, N., "Five Populations of Interplanetary Meteoroids," *Journal of Geophysical Research*, Vol. 98, No. E9, 1993, pp. 17,029–17,048.

[15]Grün, E., Staubach, P., Baguhl, M., Hamilton, D. P., "South-North and Radial Traverses Through the Interplanetary Dust Cloud," *Icarus*, Vol. 129, No. 2, 1997, pp. 270–288.

[16]Taylor, A. D., "Earth Encounter Velocities for Interplanetary Meteoroid," *Advances in Space Research*, Vol. 17, No. 12, 1996, pp. 205–209.

[17]Taylor, A. D., and Elford, W. G., "Meteoroid Orbital Element Distributions at 1 AU Deduced from the Harvard Radio Meteor Project Observations," *Earth Planets and Space*, Vol. 50, No. 6–7, 1998, pp. 569–575.

[18]Kessler, D. J., "A Guide to Using Meteoroid-Environment Models for Experiment and Spacecraft Design Applications," NASA TN D-6596, May 1972.

[19]Anderson, B. J., "Natural Orbital Environment Guidelines for Use in Aerospace Vehicle Development," NASA TM 4527, June 1994, Chap. 7.

[20]McDonnell, J. A. M., Drolshagen, G., and Gardner, D. J., "EURECA's Exposure in the Earth Space Environment," *Advances in Space Research*, Vol. 16, No. 1, 1995, pp. 73–76.

[21]Berthoud, L., and Mandeville, J. C., "Low-Earth-Orbit Micrometeoroid and Debris Investigations," *Journal of Spacecraft and Rockets*, Vol. 34, No. 1, 1997, pp. 125–132.

A. C. Tribble
Associate Editor